SDS-22 stabilizes the PP1 catalytic subunits GSP-1/-2 contributing to polarity establishment in *C. elegans* embryos

Yi Li[1], Ida Calvi[2], Monica Gotta[1*]

[1] Department of Cell Physiology and Metabolism, Faculty of Medicine, University of Geneva, Geneva 1211, Switzerland

[2] Friedrich Miescher Institute for Biomedical Research (FMI), Basel, Switzerland

*Correspondence: monica.gotta@unige.ch

Abstract

In many cells, cell polarity depends on the asymmetric distribution of the conserved PAR proteins, maintained by a balanced activity between kinases and phosphatases. The *C. elegans* one-cell embryo is polarized along the anterior-posterior axis, with the atypical protein kinase C PKC-3 enriched in the anterior, and the ring finger protein PAR-2 in the posterior. PAR-2 localization is regulated by PKC-3 and the PP1 phosphatases GSP-1/-2. Here, we find that, like GSP-2 depletion, depletion of the conserved PP1 interactor SDS-22 results in the rescue of the polarity defects of a *pkc-3* temperature-sensitive mutant. Consistent with the rescue, SDS-22 depletion or mutation results in reduced GSP-1/-2 protein levels and activity. The decreased levels of GSP-1/-2 can be rescued by reducing proteasomal activity. Our data suggest that SDS-22 regulates polarity not by directly regulating the localization or activity of GSP-1/-2, but by protecting these PP1 catalytic subunits from proteasome-mediated degradation, supporting recent data in human cells showing the SDS22 is required to stabilize nascent PP1.

Introduction

Cell polarity is crucial for cellular and tissue architecture and function. In epithelial cells, polarity specifies the apical, basal and lateral membrane domains, enabling the selective barrier function of the epithelium (Riga *et al*, 2020). In migrating cells, front-to-rear polarity is crucial for cells to respond to environmental cues such as inflammatory factors, bacterial products, or growth factors (Llense & Etienne-Manneville, 2015). Cell polarity is crucial for asymmetric cell division, which is a prerequisite for stem cells to self-renew and to generate specialized daughter cells (Santoro *et al*, 2016) and for embryos to properly develop (Campanale *et al*, 2017). In many cells, polarity is regulated by the conserved partitioning defective (PAR) proteins, which were first identified in *C. elegans* (Goldstein & Macara, 2007; Lang & Munro, 2017).

The one-cell *C. elegans* embryo is polarized along the anterior-posterior axis. The anterior PAR proteins (the PDZ proteins PAR-3 and PAR-6, the atypical protein kinase C PKC-3 and the small GTPases CDC-42) are localized to the anterior cortex and cytoplasm of the embryo, while the posterior PAR proteins (the kinase PAR-1, the ring finger protein PAR-2, the lethal giant larvae ortholog LGL-1 and the CDC-42 GAP CHIN-1) are enriched in the posterior half of the embryo (reviewed in (Goehring, 2014; Lang & Munro, 2017)). Before polarity establishment, the anterior PAR proteins are uniformly localized on the cortex, while the posterior PAR proteins are localized in the cytoplasm. Shortly after fertilization, the centrosomal mitotic kinase Aurora A (AIR-1) removes the Rho GEF ECT-2 from the posterior pole (Kapoor & Kotak, 2019; Klinkert *et al*, 2019; Longhini & Glotzer, 2022; Zhao *et al*, 2019). This event initiates a cortical flow that segregates the anterior PAR proteins to the anterior and liberates the posterior cortex of the embryo, which is then occupied by the posterior PAR proteins (Munro *et al*, 2004).

Several studies have emphasized the importance of the regulation of PAR-2 phosphorylation by PKC-3 in establishing and maintaining cortical polarity (Hao *et al*, 2006; Motegi *et al*, 2011). Recently, our group has shown that PP1 phosphatases are also required for cortical polarity in one-cell embryos (Calvi *et al*, 2022). Before polarity establishment, PKC-3 phosphorylates PAR-2 and inhibits PAR-2 localization at the cortex (Hao *et al.*, 2006; Motegi *et al.*, 2011). At polarity establishment, the PP1 phosphatases GSP-1/-2 dephosphorylate PAR-2 allowing its cortical posterior accumulation. Phosphomimetic mutants of PAR-2 (Hao *et al.*, 2006), or mutations that abolish the interaction between PAR-2 and GSP-1/-2 (Calvi *et al.*, 2022), prevent PAR-2 localization at the posterior, indicating that PP1 phosphatases are crucial for polarity establishment in *C. elegans* embryos.

Analogous to the intricate regulation of protein kinases, the activity of phosphatases towards specific substrates must be tightly regulated for proper cellular function, including cell division, heat shock

response, and glycogen metabolism (Ceulemans & Bollen, 2004). The activity of PP1 is primarily regulated post-translationally through interactions with PP1 interacting proteins, which guide its localization, substrate specificity and function. Over 200 PP1 interactors have been reported in different species and they regulate both in time and space the targeting of catalytic subunits towards different substrates (Aggen *et al*, 2000; Verbinnen *et al*, 2017; Virshup & Shenolikar, 2009). One non-canonical regulator of PP1 is the conserved SDS22 protein. In mammalian cells SDS22 suppresses Aurora B activity to control cell division (Duan *et al*, 2016; Posch *et al*, 2010; Wurzenberger *et al*, 2012). In *Drosophila melanogaster*, kinetochore-localized PP1–Sds22 dephosphorylates moesin at cell poles, facilitating anaphase elongation through polar relaxation (Rodrigues *et al*, 2015). PP1-87B and Sds22 also counteract aPKC and Aurora A kinase phosphorylation of Lgl, regulating apical-basal polarity in follicle epithelial cells (Moreira *et al*, 2019). In *Saccharomyces cerevisiae*, Sds22, along with Ypi1, is critical for the nuclear import and stabilization of PP1-Glc7 (Cheng & Chen, 2015; Peggie *et al*, 2002). Depletion of either Sds22 or Ypi1 results in mitotic arrest (Pedelini *et al*, 2007). Recent biochemical studies (Kueck *et al*, 2024) and studies in human cells (Cao *et al*, 2024) have demonstrated that SDS22 stabilizes nascent PP1 but needs to be removed from PP1 for the enzyme to be active. This underscores the complex roles of SDS22 in regulating PP1 function and reconciling the contradictory data obtained in vivo and in vitro (Cao *et al.*, 2024; Cao *et al*, 2022; Kueck *et al.*, 2024; Lesage *et al*, 2007).

In *C. elegans* GSP-1 and GSP-2, orthologues of human PP1β and PP1α, contribute to diverse processes such as germline immortality (Billmyre *et al*, 2019), sister chromatin cohesion in meiosis (Hsu *et al*, 2000; Tzur *et al*, 2012), centriole duplication (Peel *et al*, 2017), PAR-2 localization (Calvi *et al.*, 2022) in the early embryos, and the maintenance of epidermal junctions in adult worms (Beacham *et al*, 2022). Associated regulatory proteins have been identified for specific functions: for example, SDS-22 and SZY-2 modulate GSP-1 and GSP-2 activity in centriole duplication (Peel *et al.*, 2017), and APE-1 directs localization of GSP-2 to epidermal cell-cell junctions (Beacham *et al.*, 2022). However, the regulation of GSP-1 and GSP-2 during polarity establishment in one-cell embryos remains unknown.

Here we show that SDS-22 depletion rescues the polarity defects caused by reduced PAR-2 phosphorylation in the *pkc-3(ne4246)* mutant at the semi-restrictive temperature (24°C), similarly to the depletion of GSP-2. Depletion of SDS-22 results in lower GSP-1 and GSP-2 protein levels which can be rescued by depleting proteasomal subunits. These results establish SDS-22 as a regulator of PAR polarity establishment in the *C. elegans* one-cell embryo and are consistent with and complement the recent data in mammalian cells showing that SDS22 is important to control the stability of the PP1 phosphatase (Cao *et al.*, 2024).

Result

Depletion of SDS-22 suppresses polarity defects of a temperature sensitive *pkc-3* mutant

We have previously found that PP1 phosphatases GSP-1 and GSP-2 counteract the activity of the atypical protein kinase PKC-3 and allow cortical localization of PAR-2 in *C. elegans* embryos. However, the regulator(s) of GSP-1 and GSP-2 in polarity establishment is not known. In immunoprecipitations followed by mass spectrometry analysis of mNG::GSP-2 from embryos, we identified three interactors that have been previously reported as evolutionarily conserved PP1 regulators: SDS-22, APE-1 and SYZ-2(I-2) (Fig EV1).

We first asked whether depletion of any of these three regulators suppress the embryonic lethality of *pkc-3(ne4246); gfp::par-2* embryos at the semi-permissive temperature of 24°C (in which PKC-3 is partially active, temperature used in all experiments with the *pkc-3(ne4246)* mutant, unless otherwise stated), similar to depletion of the catalytic subunit GSP-2. None of these three regulators was able to suppress the embryonic lethality (Fig 1A). SDS-22 depletion alone resulted in 73.6% of embryonic lethality in the *gfp::par-2* strain, consistent with previous findings (Peel *et al.*, 2017). We then investigated if any of these regulators was able to rescue the aberrant PAR-2 localization of *pkc-3(ne4246)* embryos. Neither APE-1 nor SYZ-2 depletion rescued the symmetric PAR-2 localization observed in *pkc-3(ne4246); gfp::par-2* embryos (Fig EV2A). In contrast, depletion of SDS-22 resulted in PAR-2 localization being restricted to the posterior cortex in 87.5% of the one-cell stage embryos (Fig 1B) and PAR-2 was localized to the P1 blastomere after the first cell-division (Movie EV1). Depletion of SDS-22 in otherwise wildtype *gfp::par-2* embryos did not impair anterior-posterior polarity, with PAR-2 restricted to the posterior cortex (Fig 1B), indicating that the lethality caused by loss of SDS-22 is not the result of impaired PAR polarity establishment. However, similar to what has been observed in GSP-2 depleted embryos (Calvi *et al.*, 2022), the PAR-2 domain was smaller (Fig 1C, Fig EV2B).

We then investigated whether SDS-22 depletion, similar to GSP-2 depletion, rescued aberrant PAR-2 localization in another genetic background. When the PP1 binding motif in PAR-2 (164 RLFF 167) is optimized by a single amino acid substitution (L165V, resulting in RVFF, based on previous studies that show better binding to PP1(Meiselbach *et al*, 2006)), PAR-2 abnormally occupies the anterior cortex in early embryos. This phenotype is rescued by depletion of GSP-2, suggesting that it depends on higher activity of GSP-2 on PAR-2 (Calvi *et al.*, 2022). SDS-22 depletion also rescued the anterior PAR-2 domain observed in *gfp::par-2(L165V)* embryos as anterior PAR-2 was observed in only 45.5% of *gfp::par-2(L165V); sds-22(RNAi*) embryos compared to 100% *gfp::par-2(L165V); ctrl(RNAi*) embryos (Fig EV3).

Polarity controls the posterior positioning of the mitotic spindle, which results in an asymmetric cell division producing a larger anterior AB cell and a smaller posterior P1 cell. In *gfp::par-2* embryos AB cell accounts for 56.5% of the total embryo length. In contrast, polarity defects in the *pkc-3(ne4246)*

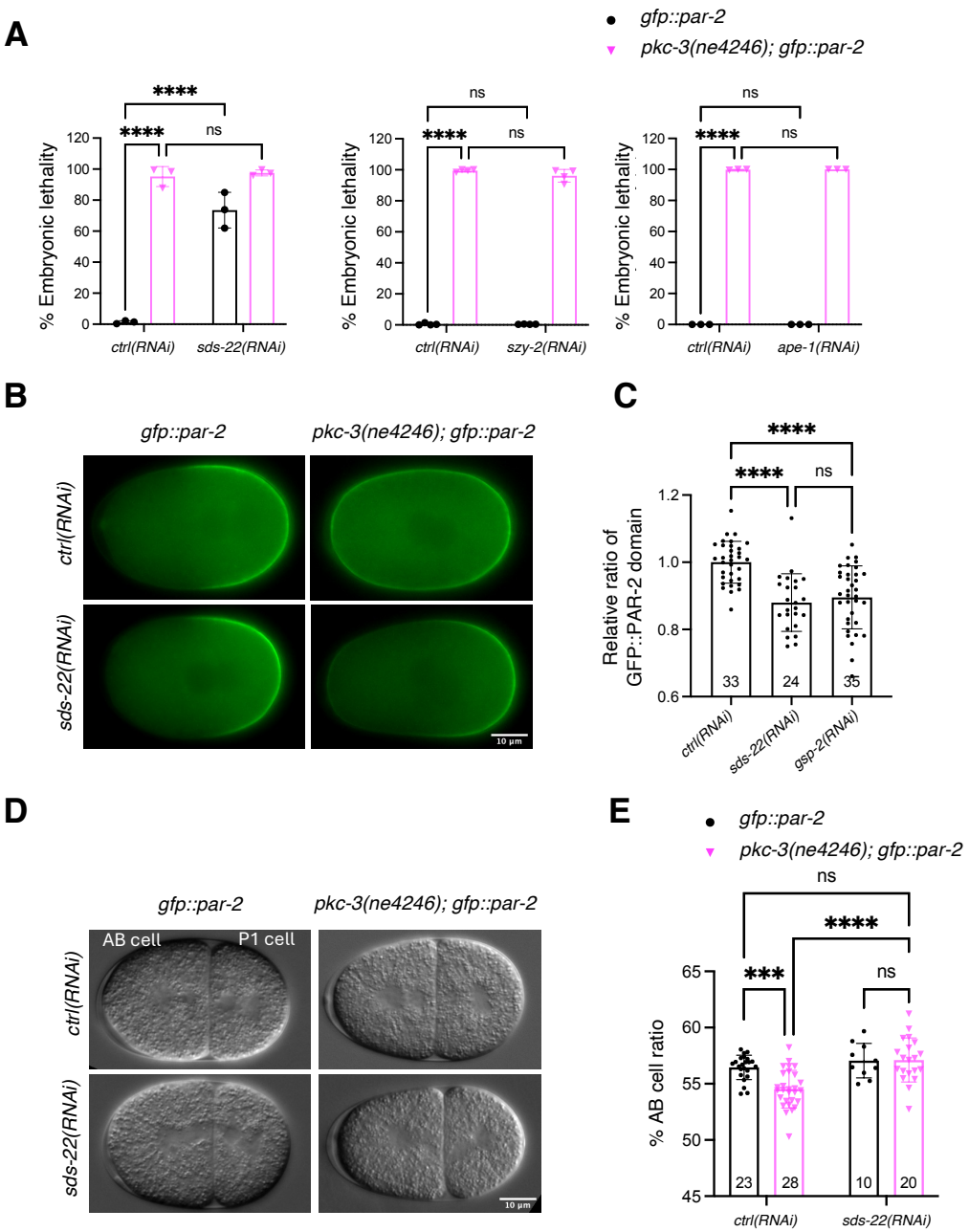

Fig 1: SDS-22 depletion suppresses the polarity defects of the *pkc-3(ne4246)* mutant. **(A)** Embryonic lethality of *gfp::par-2* and *pkc-3(ne4246); gfp::par-2* embryos with the indicated depletions. The reported values correspond to the percentage of unhatched embryos over the total progeny (larvae and unhatched embryos) in all figures. *gfp::par-2; ctrl(RNAi)*, *n* = 4,975, *gfp::par-2; sds-22(RNAi)*, *n* = 3,923, *pkc-3(ne4246); gfp::par-2; ctrl(RNAi)*, *n* = 2,247, and *pkc-3(ne4246); gfp::par-2; sds-22(RNAi)*, *n* = 1,611. *gfp::par-2; szy-2(RNAi)*, *n* = 3,550; *pkc-3(ne4246); gfp::par-2; szy-2(RNAi)*, *n* = 2,588. *gfp::par-2; ape-1(RNAi)*, *n* = 720; *pkc-3(ne4246); gfp::par-2; ape-1(RNAi)*, *n* = 930. *sds-22(RNAi)* and *ape-1(RNAi), N* = 3. *szy-2(RNAi), N* = 4. The mean is shown and error bars indicate Standard Deviation (SD). The P values were determined using two-way ANOVA Tukey's multiple comparisons test. For plots of embryonic lethality, each dot inside the bar represents the average lethality of each independent experiment, unless otherwise indicated. **(B)** Representative frames of time-lapse videos of embryos at the pronuclear meeting stage: *gfp::par*-2; *ctrl(RNAi)*, *n* = 12 (PAR-2 is posterior in 100% of them), *gfp::par-2; sds-22(RNAi), n* = 12 (100% posterior PAR-2), *pkc-3(ne4246); gfp::par-2; ctrl(RNAi), n* = 42 (0% posterior PAR-2, PAR-2 is all around the cortex in all

155 of them), and *pkc-3(ne4246); gfp::par-2; sds-22(RNAi)*, n = 48 (87.5% have PAR-2 restricted to the
156 posterior cortex). N = 5. **(C)** Quantification of the GFP::PAR-2 domain size at pronuclear meeting in
157 live embryos with the indicated RNAi conditions. Sample size (n) is indicated inside the bars in the
158 graph. N = 4. Mean is shown and error bars indicate SD. The P values were determined using one-way
159 ANOVA. In C and E, each dot represents a single embryo. **(D)** Still images of two-cell embryos of the
160 indicated genotypes taken from DIC time-lapse movies. **(E)** Quantification of the AB cell size as a
161 percentage of the whole embryo size. Sample size (n) is indicated inside the bars in the graph. N = 3.
162 Mean is shown and error bars indicate SD. The P-values were determined using two-way ANOVA
163 "Tukey's multiple comparisons test". For all the panels, RNA interference was performed by feeding.
164 Scale bar is 10 µm, anterior is to the left and posterior to the right. In all plots, ns $p > 0.05$, * $p < 0.05$,
165 ** $p < 0.01$, ***$p < 0.001$, ****$p < 0.0001$, n = number of embryos analyzed; N = number of
166 independent experiments.
167
168 mutant lead to reduced cell size asymmetry with a smaller AB cell, occupying 54.2% of the embryo
169 length. Consistent with the suppression of PAR-2 polarity defect, depletion of SDS-22 in *pkc-3(ne4246)*
170 embryos resulted in a bigger AB cell (57.1% embryo length), comparable to the size of AB in control
171 *gfp::par-2* embryos (Fig 1D,E).
172 Our data show that depletion of SDS-22 results in a smaller PAR-2 domain, suppresses the polarity
173 defects of a *pkc-3* temperature sensitive strain and the aberrant PAR-2 localization observed in the PAR-
174 2(L165V) mutant strain. As SDS-22 is a conserved PP1 regulator, our data suggest that SDS-22
175 positively regulates GSP-2 in polarity establishment.
176
177 **The conserved E153 of SDS-22 is important for SDS-22 interaction with GSP-1 and GSP-2**
178 We have identified SDS-22 in immunoprecipitation with GSP-2 from embryos, thereby confirming a
179 previous finding that SDS-22 immunoprecipitates with both GSP-1 and GSP-2 from full worm lysates
180 (Peel *et al.*, 2017). We were able to confirm the interaction of SDS-22 with both GSP-1 and GSP-2 in
181 a two-hybrid assay (Fig 2).
182 SDS-22 is a leucine-rich repeat (LRR) protein and does not contain the degenerate RLxF PP1 docking
183 motif that has been found in most PP1 regulators. Instead, a conserved glutamic acid E153 in the LRR
184 domain is important for its interaction with the PP1 catalytic subunits (Fig 2) (Ceulemans *et al*, 2002;
185 Eiteneuer *et al*, 2014; Heroes *et al*, 2019). This site is conserved in *C. elegans* and we asked whether it
186 is important for the interaction of SDS-22 with GSP-1and GSP-2. Substitution of the glutamine E153
187 with Alanine (referred to as SDS-22(E153A)) abrogated the interaction with both GSP-1 and GSP-2 in
188 the two-hybrid assays (Fig 2).
189 These data confirm that SDS-22 interacts with both GSP-1 and GSP-2 and identify the glutamic acid
190 residue E153 in the LRR domain of SDS-22 as crucial for the interaction, consistent with what has been
191 demonstrated for the human orthologs (Ceulemans *et al.*, 2002; Eiteneuer *et al.*, 2014; Heroes *et al.*,
192 2019).
193

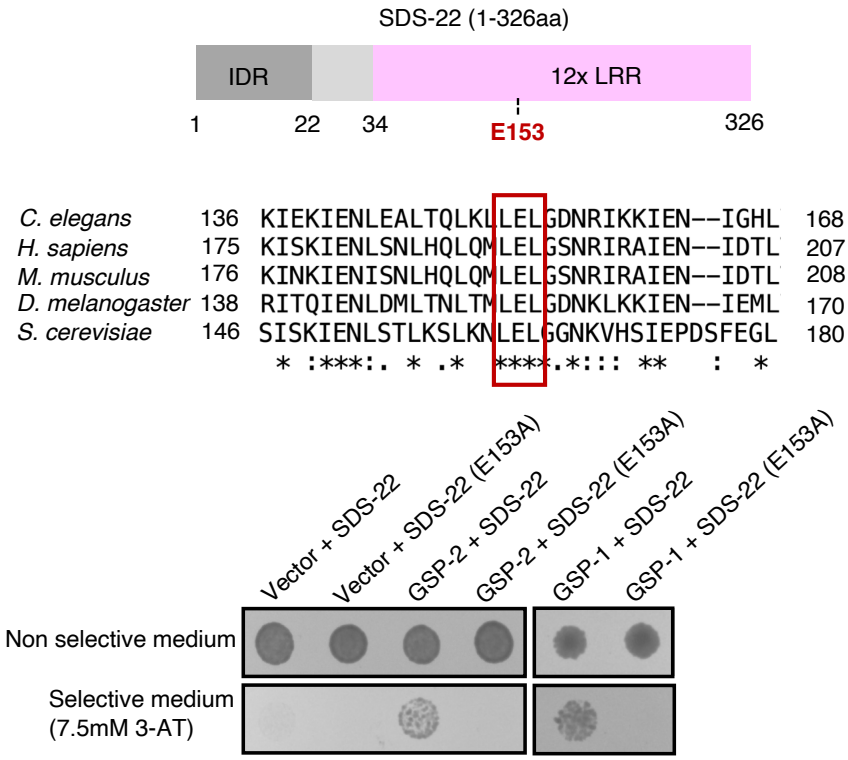

Fig 2: SDS-22 interacts with GSP-1 and GSP-2 via the conserved E153 residue.
Upper panel: schematic representation of the full-length (1-326aa) SDS-22. IDR: intrinsically disordered region; LRR: leucine-rich repeats; E153: glutamic acid at amino acid residue 153. Middle panel: sequence alignment of one PP1 interacting region in SDS22 from *C. elegans* (Uniprot P45969), *H. sapiens* (Uniprot Q15435), *M. musculus* (Uniprot Q3UM45), *D. melanogaster* (Uniprot Q9VEK8), and *S. cerevisiae* (Uniprot 936047). The reported PP1-binding residue E192 of *H. sapiens* is present in *C. elegans* as E153, and this site is conserved in all species listed (marked by red square). Figure adapted from alignment obtained with Uniprot alignment tool (https://www.uniprot.org/align). Lower panel: yeast two-hybrid assays showing the interaction between SDS-22 (wild type and the E153A mutant) and GSP-1 and GSP-2. Yeasts were transformed with the indicated plasmids (SDS-22 and SDS-22(E153A) are fused to the DNA Binding Domain and GSP-1 and GSP-2 to the Activation Domain) and were grown on non-selective and selective medium. Interaction between bait and prey results in growth on selective medium (7.5mM 3-AT).

Polarity defects are rescued in *pkc-3(ne4246); sds-22(E153A); gfp::par-2* embryos

Our two-hybrid data show that SDS-22 interacts with GSP-1 and GSP-2 through the E153 residue. We introduced this substitution in vivo and asked whether *sds-22(E153A)* mutant embryos display a shorter PAR-2 domain, as observed in SDS-22 depleted embryos (Fig 1B,C). PAR-2 was restricted to the posterior in *gfp::par-2; sds-22(E153A)* as in control embryos, but the length of the domain was decreased (Fig 3A,B, Movie EV2), similar to what was observed in SDS-22 depleted embryos. However, while SDS-22 depletion resulted in 73.6% embryonic lethality (Fig 1A), *gfp::par-2; sds-22(E153A)* only exhibited 5.3% embryonic lethality compared to *gfp::par-2* strain (Fig 3C).

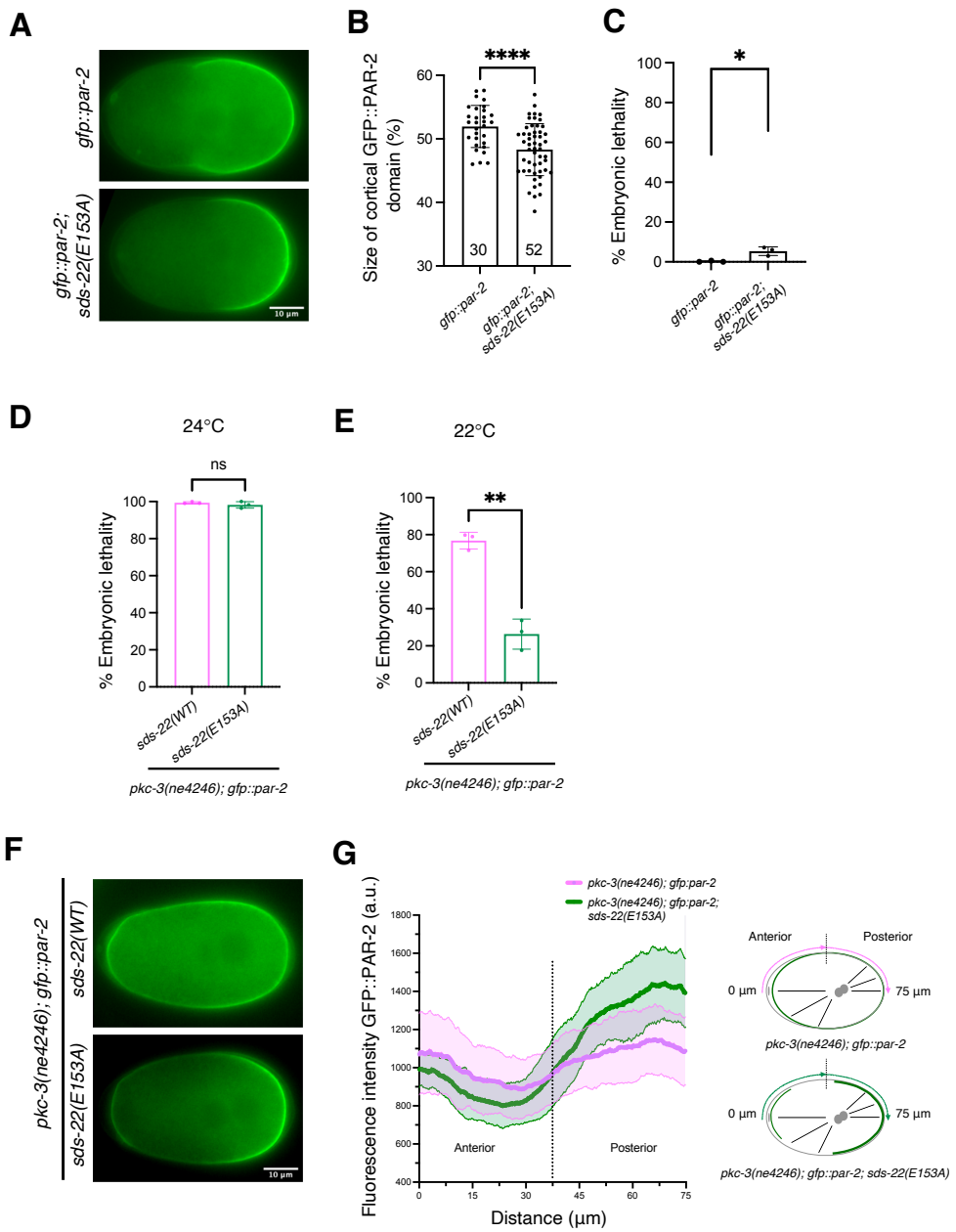

Fig 3: Mutation of SDS-22 E153 residue rescues polarity defects of *pkc-3(ne4246)* mutant. **(A)** Still images at the pronuclear meeting stage from time-lapse videos of *gfp::par-2* and *gfp::par-2; sds-22(E153A)*. **(B)** Quantification of the GFP::PAR-2 domain size at pronuclear meeting in live zygotes. Sample size (*n*) is indicated inside the bars in the graph, each dot represents a single embryo. *N* = 3. Mean is shown and error bars indicate SD. The P value was determined using two-tailed unpaired Student's *t* test. **(C)** Percentage of embryonic lethality of *gfp::par-2* and *gfp::par-2; sds-22(E153A). gfp::par-2, n* = 757, *gfp::par-2; sds-22(E153A), n* = 2644. *N* = 3. Mean is shown and error bars indicate SD. The P value was determined using two-tailed unpaired Student's *t* test. **(D, E)** Percentage of embryonic lethality of *pkc-3(ne4246); gfp::par-2* and *pkc-3(ne4246); gfp::par-2; sds-22(E153A)* at the semi-permissive temperature of 24°C **(D)** and of 22°C **(E)**. For **(D)**, *pkc-3(ne4246); gfp::par-2*, *n* = 569, and *pkc-3(ne4246); gfp::par-2; sds-22(E153A), n* = 545. For **(E)**, *pkc-3(ne4246); gfp::par-2*, *n* = 2171, and *pkc-3(ne4246); gfp::par-2; sds-22(E153A) n* = 1867. *N* = 3. Mean is shown and error bars indicate SD. The P value was determined using two-tailed unpaired Student's *t* test. In C, D and E, dots represent the mean lethality of each independent experiment. **(F)** Still images from time-lapse videos of *pkc-3(ne4246); gfp::par-2* and *pkc-3(ne4246); gfp::par-2; sds-22(E153A)* embryos at the pronuclear meeting stage. Worms were grown at the semi-permissive temperature of 22°C as in panel E. **(G)**

GFP::PAR-2 intensity line profile along half of the embryo cortex starting from the anterior, as shown in the scheme on the right. *pkc-3(ne4246); gfp::par-2* and *pkc-3(ne4246); gfp::par-2; sds-22(E153A)* $n = 19$ for both genotypes. $N = 3$. Worms were grown at the semi-permissive temperature of 22°C as in panel E and F. Scale bar is 10 µm, anterior is to the left and posterior to the right. In all plots, ns $p > 0.05$, * $p < 0.05$, ** $p < 0.01$, ***$p < 0.001$, ****$p < 0.0001$, n = number of embryos analyzed; N = number of independent experiments.

We next asked whether *sds-22(E153A)* was able to rescue the lethality and the polarity defects of *pkc-3(ne4246)* embryos. We introduced the E153A mutation in *pkc-3(ne4246); gfp::par-2* strain, let them grow at the semi-permissive temperature (24°C) and quantified embryonic lethality. We found that the lethality of the embryos was not rescued at this temperature (Fig 3D). Decreasing the temperature to 22°C reduced the embryonic lethality in the *pkc-3(ne4246); gfp::par-2* strain (Fig 3E) to about 76.8%. In these more permissive conditions, *pkc-3(ne4246); sds-22(E153A); gfp::par-2* exhibited only 26.4% embryonic lethality, indicating that the *sds-22(E153A)* mutation, which abolishes SDS-22 interaction with GSP-1/-2, can rescue the lethality of *pkc-3(ne4246)* at this temperature.

When we looked at polarity we found that PAR-2, despite still weakly detectable at the anterior, was more enriched at the posterior cortex in the *pkc-3(ne4246); sds-22(E153A); gfp::par-2* mutant embryos compared to *pkc-3(ne4246); gfp::par-2* (Fig 3F,G, Movie EV 3). The rescue of embryonic lethality and polarity phenotypes was not due to a reduced expression level of SDS-22(E153A) because SDS-22(E153A)::GFP showed similar protein intensity as SDS-22::GFP (Fig EV4).

Our data show that a mutation that disrupts the interaction of SDS-22 with GSP-1 and GSP-2 in a two-hybrid assay, can lead to a partial rescue of the lethality and the polarity defect of *pkc-3(ne4246); gfp::par-2* embryos, suggesting that the interaction of SDS-22 with the PP1 phosphatases is important for polarity establishment.

Loss or mutation of SDS-22 results in hyper-phosphorylation of a PP1 substrate

In *C. elegans* embryos GSP-1 and GSP-2 redundantly regulate PAR-2 localization (Calvi *et al.*, 2022). GSP-2 is the predominant PP1 phosphatase that allows for PAR-2's localization to the posterior cortex. Depletion of GSP-2 reduces the size of PAR-2 domain in the *gfp::par-2* strain while depletion of GSP-1 does not lead to observable defects in PAR-2 domain size. Only when GSP-1 and GSP-2 are co-depleted, PAR-2 remains mostly cytoplasmic (Fig 4A, (Calvi *et al.*, 2022)). If SDS-22 was essential to regulate the activity of both GSP-1 and GSP-2, its depletion should result in a loss of PAR-2 cortical localization, similar to what is observed in the co-depletion of GSP-1 and GSP-2. As shown above, depletion of SDS-22 in the *gfp::par-2* strain did not lead to cytoplasmic localization of PAR-2 (Fig 1B, C and 4A) but resulted in a smaller PAR-2 domain (Fig 1C and 4B), as observed in the GSP-2 depletion.

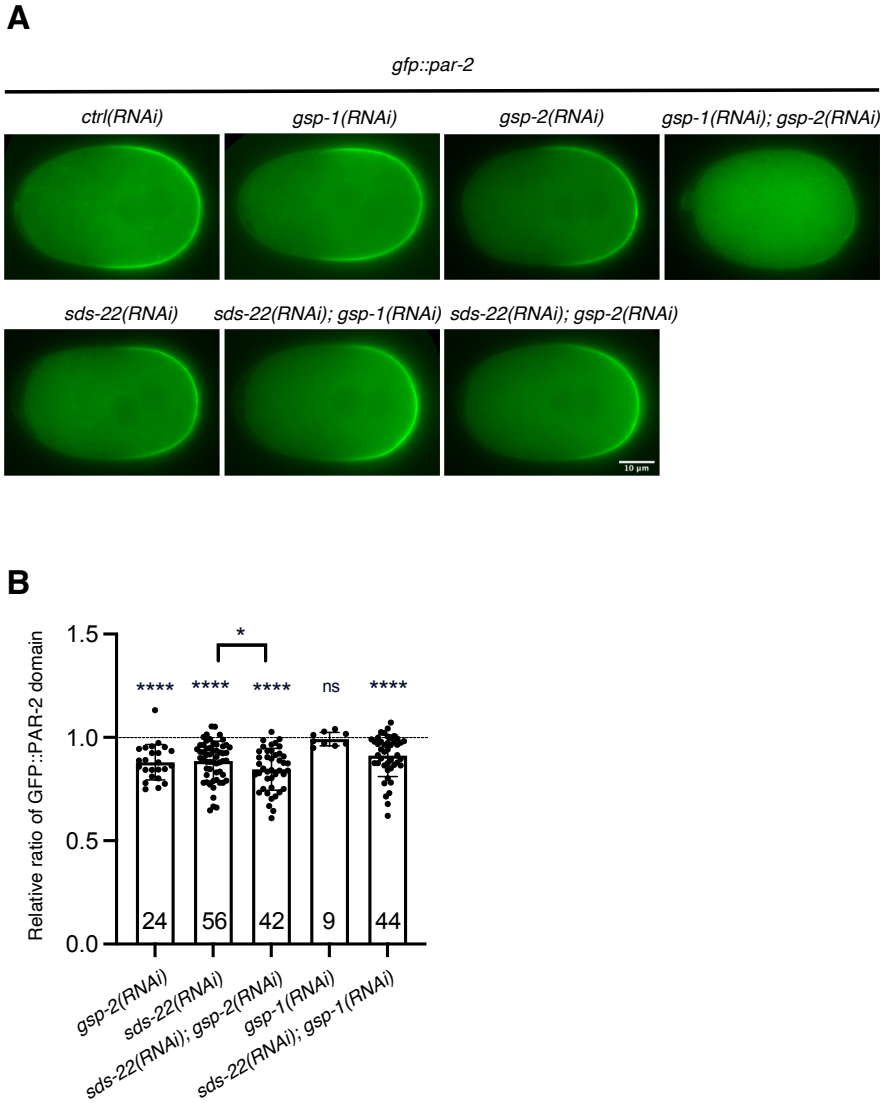

Fig 4: SDS-22 does not genetically regulate GSP-1, GSP-2 or both.
(A) Still images from time-lapse videos of *gfp::par-2* zygotes at pronuclear meeting with the indicated depletions. RNA interference was performed by injection. Scale bars is 10 µm, anterior is to the left and posterior to the right. **(B)** Quantification of the relative ratio of GFP::PAR-2 size domain with indicated RNAi conditions. Each condition was compared to *ctrl(RNAi)* treatment within the same experiment. The P value was determined using two-tailed unpaired Student's *t* test. Sample size (*n*) is indicated inside the bars in the graph. $N = 4\text{-}5$. Mean is shown and error bars indicate SD. ns $p > 0.05$, * $p < 0.05$, ** $p < 0.01$, ***$p < 0.001$, ****$p < 0.0001$.

This suggests that SDS-22 regulates GSP-2 rather than GSP-1. If this was true, depletion of both SDS-22 and GSP-1 should result in PAR-2 remaining in the cytoplasm, similar to GSP-1 and GSP-2 co-depletion. We therefore co-depleted SDS-22 and GSP-1 and, as control, SDS-22 and GSP-2. The double depletion was efficient as shown in Fig EV5. In embryos co-depleted of SDS-22 and GSP-1, PAR-2 still formed a posterior cortical domain. Co-depletion of SDS-22 and GSP-2 resulted in an even more pronounced reduction of PAR-2 domain compared to the single depletion of SDS-22 (Fig 4A,B), suggesting that SDS-22 plays a different role than simply activating GSP-2 (see below).

286 Our findings show that depletion or mutation of SDS-22 rescues polarity defects of the *pkc-3(ne4246)*
287 mutant. However, neither SDS-22 depletion alone nor co-depletion with GSP-1 or GSP-2 prevents
288 PAR-2 cortical localization similar to GSP-1/-2 co-depletion. To understand the role of SDS-22 in the
289 regulation of GSP-1 and GSP-2 and in polarity establishment, we investigated whether SDS-22
290 depletion or mutation decreases PP1 activity. To quantify the activity of the PP1 phosphatase, we
291 examined the phosphorylation levels of a well characterized substrate, histone H3, as previously
292 described (Hsu *et al.*, 2000; Qian *et al*, 2011). Histone H3 is phosphorylated at the Ser 10 residue by
293 the Aurora B kinase in the early phases of mitosis and it is dephosphorylated by PP1 at anaphase (Xin
294 *et al*, 2020). We found that phospho-histone H3 (Ser10) levels on the chromosomes during anaphase
295 were higher in SDS-22 depleted one-cell embryos (Fig 5A) compared to control depletion, indicating
296 that depletion of SDS-22 leads to deficient dephosphorylation of PP1 substrates.

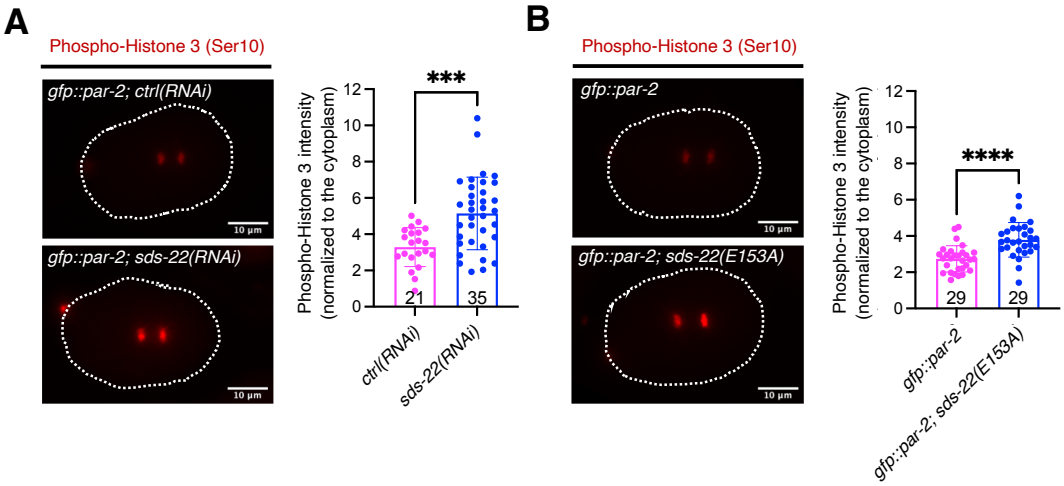

297

298 **Fig 5. Loss or mutation of SDS-22 decreases GSP-1 and GSP-2 activity.**
299 **(A)** Left, images of a *gfp::par-2; ctrl(RNAi)* anaphase embryo and a *gfp::par-2; sds-22(RNAi)* anaphase
300 embryo stained for phospho-histone H3 (Ser10) (in red). Right, quantifications. **(B)** Left, images of a
301 *gfp::par-2* and a *gfp::par-2*; *sds-22(E153A)* embryo at anaphase stained for phospho-histone H3(Ser10)
302 (in red). Right, quantifications. For both **A** and **B**, sample size (*n*) is indicated inside the bars in the
303 graph, each dot represents an embryo. $N = 4$. Phospho-histone H3 (Ser10) intensity was normalized to
304 cytoplasmic levels. The P-values were determined using two-tailed unpaired Student's t-test. ***$p <$
305 0.001, ****$p < 0.0001$. The dashed lines indicate the outline of embryos. RNA interference was
306 performed by feeding. Scale bar is 10 µm.
307

308 Similar to the observation in SDS-22 depleted embryos (Fig 5A), phospho-histone H3 (Ser10) levels
309 were higher in the *sds-22(E153A)* mutant embryos (Fig 5B), suggesting that the interaction between
310 SDS-22 and GSP-1 and GSP-2 is important to maintain efficient dephosphorylation of a PP1 substrate.
311 To conclude, while our genetic data on PAR-2 cortical localization suggest that SDS-22 is not required
312 to fully activate GSP-1 and/or GSP-2, depletion or mutation of SDS-22 results in a reduced activity of
313 the phosphatases.
314

315 **SDS-22 maintains GSP-1 and GSP-2 protein levels by protecting them from proteasomal**
316 **degradation**
317 Regulatory subunits of phosphatases can regulate their activity, localization or protein levels (Aggen *et*
318 *al.*, 2000; Verbinnen *et al.*, 2017; Virshup & Shenolikar, 2009). Recent work in human cells and in
319 vitro has shown that SDS22 coordinates the assembly of the PP1 holoenzyme (Cao *et al.*, 2024; Kueck
320 *et al.*, 2024). To understand how SDS-22 contributes to the function of GSP-1 and GSP-2, we
321 investigated whether SDS-22 regulated the localization or levels of GSP-1 and GSP-2. We depleted
322 SDS-22 in the *mNG::gsp-2* and *gfp::gsp-1* strains and observed that the localization of GSP-2 and GSP-
323 1 was not altered by SDS-22 depletion (Fig 6A). However, the intensity of mNG::GSP-2 and
324 GFP::GSP-1 dropped to 53.7% and 59.5% compared to the control strains (Fig 6B,C). This result was
325 confirmed by western blot analysis (Fig 6D,E). SDS-22 is therefore essential to maintain the proper
326 levels of GSP-1 and GSP-2 in *C. elegans* embryos.
327 We next asked whether SDS-22 maintains GSP-1 and GSP-2 levels in vivo via their physical interaction
328 with the proteins. We generated strains in which the E153 site of SDS-22 is mutated in the genetic
329 background of *mNG::gsp-2* and *gfp::gsp-1* separately. In contrast to the low lethality observed in
330 *sds-22(E153A)* mutant in the *gfp::par-2* genetic background (Fig 3C), *sds-22(E153A)* mutation caused
331 99.1% embryonic lethality in *mNG::gsp-2* and 32.3% in *gfp::gsp-1* (Fig EV6A,B). These data suggest
332 that tagged GSP-2 and GSP-1 strains are hypomorph even though there are no observable growth
333 defects nor embryonic lethality in these strains. Because of the high embryonic lethality of *mNG::gsp-*
334 *2; sds-22(E153A)* homozygous mutant, we maintained the strain as a *sds-22(E153A)* heterozygote (see
335 methods). Consistent with the phenotypes of *sds-22(RNAi)*, SDS-22(E153A) mutation led to a 46.3%
336 of reduction of the mNG::GSP-2 intensity (Fig 6F,G) and to a 21% reduction of the GFP::GSP-1
337 intensity (Fig 6F,H).
338 We then investigated whether the levels of GSP-1 and/or GSP-2 affected the levels of SDS-22. We
339 performed single depletion and co-depletion of GSP-1 and GSP-2 in *sds-22::gfp* strain. We found that
340 the levels of SDS-22 were weakly reduced by single depletion of GSP-1 or GSP-2 (around 8% of
341 reduction in both conditions), but were un-affected by co-depletion of both GSP-1 and GSP-2 (Fig
342 EV7A,B).
343
344
345
346

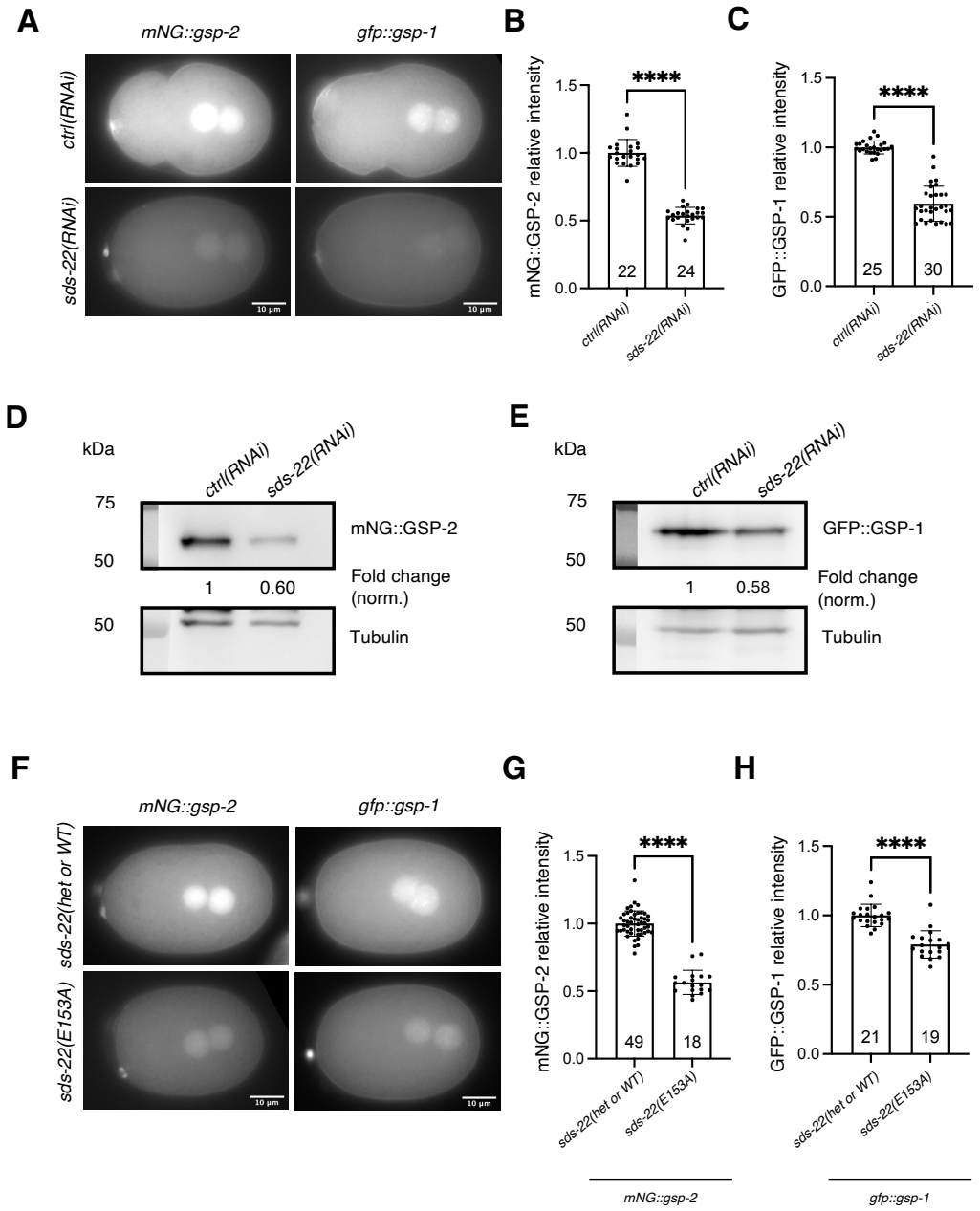

Fig 6: SDS-22 depletion or mutation causes a reduction of GSP-1 and GSP-2 protein levels. **(A)** Representative images of *mNG::gsp-2* and *gfp::gsp-1* embryos in *ctrl(RNAi)* and *sds-22(RNAi)*. **(B, C)** Quantification of relative mNG::GSP-2 **(B)** and GFP::GSP-1 **(C)** levels in *sds-22(RNAi)* normalized to *ctrl(RNAi)*. Mean is shown and error bars indicate SD. $N = 4$. ****$p < 0.0001$. **(D, E)** Western Blot of embryonic extracts from *mNG::gsp-2* **(D)** and *gfp::gsp-1* **(E)** in *ctrl(RNAi)* and *sds-22(RNAi)* embryos. Tubulin is used as a loading control. Fold change of mNG::GSP-2 and GFP::GSP-1 normalized to Tubulin levels were shown below the Western blot image. $N = 1$. **(F)** Representative images of *mNG::gsp-2; sds-22(E153A/+ or +/+,* a mixture of wild type and heterozygous of the E153A mutant, see methods), *mNG::gsp-2; sds-22(E153A), gfp::gsp-1* and *gfp::gsp-1; sds-22(E153A).* **(G, H)** Quantification of relative mNG::GSP-2 **(G)** and GFP::GSP-1 **(H)** levels with SDS-22(E153A) mutation normalized to wild type. *mNG::gsp-2,* $N = 3$. *gfp::gsp-1,* $N = 4$. ****$p < 0.0001$. In A-E, RNA interference was performed by feeding. In **B**, **C**, **G**, **H**, mean is shown, error bars indicate SD, the P-values were determined using two-tailed unpaired Student's t-test. Dots in graphs represent individual embryo measurements and sample size (*n*) is indicated inside the bars in the graph.

362 In budding yeast, when Sds22 is mutated, PP1-Glc7 is prone to misfold and form aggregates with heat-
363 shock proteins, which are cleared by the proteasome (Cheng & Chen, 2015). Additionally, in human
364 cells, SDS22 stabilizes nascent PP1 (Cao *et al.*, 2024). We hypothesized that GSP-1 and GSP-2 are
365 degraded by the proteasome when SDS-22 is depleted or mutated. To test this hypothesis, we reduced
366 proteasomal activity in SDS-22-depleted or mutated embryos by depleting the proteasomal subunits
367 RPN-6.1 or RPN-7, which localize to the 19S regulatory complex and are essential for the proteolytic
368 activity (Fernando *et al*, 2022; Papaevgeniou & Chondrogianni, 2014). Since depletion of these subunits
369 results in sterile worms, we analyzed the protein intensity of GSP-1 and GSP-2 in the -1 and -2 oocytes
370 in the germline and investigated whether reducing proteasomal activity would restore GSP-1 and GSP-2
371 levels.
372 When RPN-6.1 or RPN-7 were depleted, there was an increase of GSP-1 and GSP-2 intensity both in
373 the cytoplasm and in the nucleus of the oocytes (Fig 7A-F, Fig EV8), indicating that GSP-1 and GSP-
374 2 are subject to proteasomal degradation in the germline of *C. elegans*. Consistent with the observation
375 in embryos (Fig 6A), both cytoplasmic and nuclear GSP-2 levels in the germline were reduced by about
376 50% after depletion of SDS-22 (Fig 7B,C). Importantly, when SDS-22 was depleted together with
377 RPN-6.1 or RPN-7, the level of GSP-2 was restored (Fig 7A-C, Fig EV8A). The efficiency of SDS-22
378 depletion in the RPN-6.1 or RPN-7 co-depletion was verified (Fig EV9). In *sds-22(RNAi)* oocytes, the
379 levels of GFP::GSP-1 exhibited a smaller decrease (17.4%) in the nucleus and an even smaller reduction
380 in the cytoplasm, which was not statistically significant (8.8%, n.s.) (Fig 7D-F). The reduced nuclear
381 and cytoplasmic intensities of GSP-1 following SDS-22 depletion were also rescued by co-depletion of
382 RPN-6.1 or RPN-7 (Fig 7D-F, Fig EV8B), similar to the recovery of GSP-2 levels (Fig 7B,C). To
383 further test the role of SDS-22 on GSP-1 stability, we measured GFP::GSP-1 levels in the -1 and -2
384 oocytes in the *gfp::gsp-1; sds-22(E153A)* strain. In the germline of *gfp::gsp-1; sds-22(E153A)* worms,
385 GSP-1 levels were reduced (28.8% in the cytoplasm; 31.0% in the nucleus) (Fig 7G-I). In the same
386 mutant, depletion of RPN-6.1 or RPN-7 increased the levels of GSP-1 (Fig 7G-I, Fig EV8C), supporting
387 our hypothesis that SDS-22, through its interaction with GSP-1, protects GSP-1 from proteasome
388 mediated degradation. Adult *mNG::gsp-2; sds-22(E153A)* homozygote worms only produced dead
389 embryos (Fig EV6A), precluding the possibility to analyze their germlines with depletion of RNP-6.1
390 or RPN-7.
391 In summary, our results show that SDS-22 maintains the levels of GSP-1 and GSP-2 by protecting them
392 from proteasome mediated degradation.

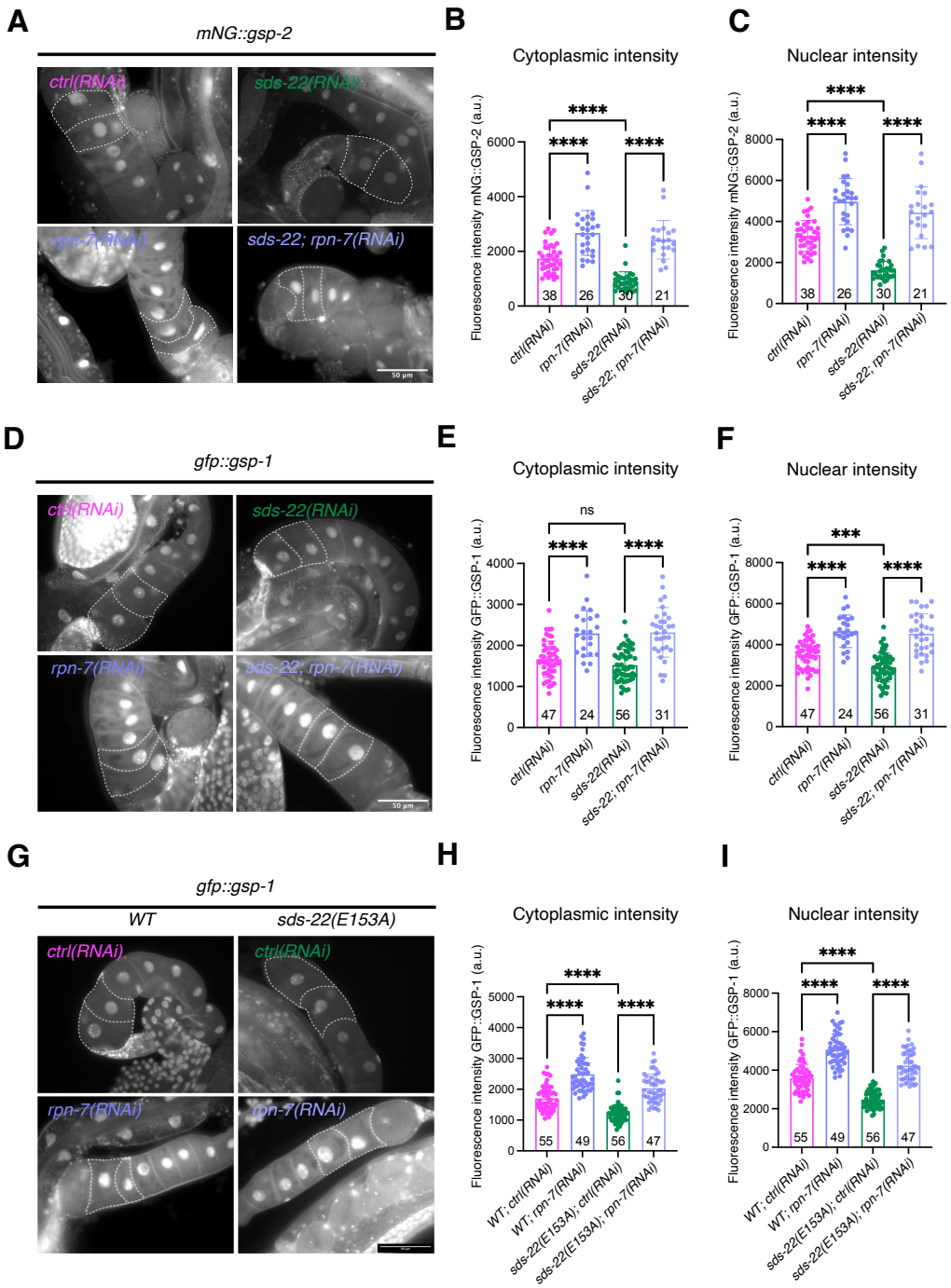

Fig 7: SDS-22 protects GSP-1 and GSP-2 from proteasomal degradation.
(A) Representative images of *mNG::gsp-2* germlines in *ctrl(RNAi), sds-22(RNAi), rpn-7(RNAi)* and *sds-22(RNAi); rpn-7(RNAi)*. **(B, C)** Quantification of mNG::GSP-2 intensity levels in the cytoplasm **(B)** and nucleus **(C)** of -1 and -2 oocytes. $N = 3$. **(D)** Representative images of *gfp::gsp-1* germlines in *ctrl(RNAi), sds-22(RNAi), rpn-7(RNAi)* and *sds-22(RNAi); rpn-7(RNAi)*. **(E, F)** Quantification of GFP::GSP-1 intensity levels in the cytoplasm **(E)** and nucleus **(F)** of -1 and -2 oocytes. $N = 3$. **(G)** Representative midsection images of *gfp::gsp-1, gfp::gsp-1;sds-22(E153A)* germlines in *ctrl(RNAi)* and *rpn-7(RNAi)*. **(H, I)** Quantification of GFP::GSP-1 intensity levels in the cytoplasm **(H)** and nucleus **(I)** of -1 and -2 oocytes. $N = 3$. For **B**, **C**, **E**, **F**, **H** and **I**, mean is shown and error bars indicate SD. Each dot represents the measurement of one germline. The P-values were determined using one-way ANOVA "Tukey's multiple comparisons test". Sample size (n) is indicated inside the bars in the graph. For all panels, RNA interference was performed by feeding. The scale bars are 50 µm. In all plots, ns $p > 0.05$, * $p < 0.05$, ** $p < 0.01$, ***$p < 0.001$, ****$p < 0.0001$, n = number of embryos analyzed; N = number of independent experiments.

408 **Discussion**
409
410 Cell polarity establishment in the *C. elegans* embryos is crucial for subsequent asymmetric cell
411 divisions and later development. Previous studies have shown that the balanced activity of the kinase
412 PKC-3 and the PP1 phosphatases GSP-1 and GSP-2 is essential for the posterior cortical localization
413 of PAR-2 (Calvi *et al.*, 2022; Hao *et al.*, 2006; Motegi *et al.*, 2011). GSP-1/-2 are PP1 catalytic subunits
414 that rely on regulatory subunits to direct their cellular localization or facilitate their activity within a
415 functional holoenzyme. Here, we demonstrate that a conserved PP1 regulator, SDS-22, contributes to
416 the activity of GSP-1/-2 by protecting them from proteasomal degradation and maintaining their protein
417 levels. Depletion of SDS-22, or mutation of its E153 residue (E153A) important for SDS-22-PP1
418 interaction resulted in reduced GSP-1/-2 protein levels, decreased dephosphorylation of a PP1 substrate,
419 and a smaller PAR-2 domain, suggesting that SDS-22 regulates GSP-1/-2 activity to control the loading
420 of PAR-2 to the posterior cortex in one-cell stage *C. elegans* embryos.
421 SDS-22 is a conserved protein previously shown to be important for cell polarity. In *Drosophila,* Sds22
422 is essential for maintaining the morphology and apical-basal polarity of follicle epithelial cells (Grusche
423 *et al*, 2009) and it facilitates the cortical localization of the lethal giant larvae (Lgl) protein in these cells
424 (Moreira *et al.*, 2019). In mammalian and yeast cells, SDS22 has been shown to be essential for mitotic
425 progression (Duan *et al.*, 2016; Posch *et al.*, 2010; Wurzenberger *et al.*, 2012). Even though SDS22
426 appears as a conserved regulator of PP1 phosphatases, the exact mechanism by which SDS22 regulates
427 PP1 activity was still debated. Some studies have shown that SDS22 positively contributes to PP1
428 activity in mitosis (MacKelvie *et al*, 1995; Stone *et al*, 1993) and plays a role in localizing PP1 and in
429 protein folding of the PP1 complex (Cheng & Chen, 2015; Peggie *et al.*, 2002). However, other studies
430 suggested that SDS22 inhibits PP1 activity in vitro (Lesage *et al.*, 2007). Two recent studies from the
431 Bollen and Meyer groups show that SDS22 plays a key role in the biogenesis of PP1 holoenzymes (Cao
432 *et al.*, 2024; Kueck *et al.*, 2024). On the one hand, SDS22 stabilizes newly translated PP1; on the other
433 hand, SDS22 and Inhibitor 3 (I3) bind to PP1, forming a ternary complex that inhibits PP1 activity.
434 This inhibitory complex is dissociated by the AAA ATPase p97/Valosin, allowing PP1 to bind
435 canonical regulatory subunits to form a functional holoenzyme. These data reconcile the contradictory
436 in vivo and in vitro observations.
437 Our data in *C. elegans* support and complement these studies. We show that SDS-22 is not essential for
438 full activation of both GSP-1 and GSP-2, since depletion of SDS-22 does not abolish polarity, as
439 observed in the co-depletion of GSP-1 and GSP-2 (Calvi *et al.*, 2022). Embryos co-depleted of SDS-22
440 and GSP-1 or of SDS-22 and GSP-2, are also able to polarize, indicating that SDS-22 plays a different
441 role than simply activating GSP-1, GSP-2 or both. We find that in *C. elegans* SDS-22 is required to
442 maintain the appropriate levels of both GSP-1 and GSP-2. This finding explains why loss of SDS-22,
443 similar to GSP-2 depletion, rescues PAR-2 defect in *pkc-3(ne4246)* mutant allele (Fig 1B), while
444 embryos are still able to polarize after single depletion of SDS-22, or co-depletion of SDS-22 with GSP-

445 1 or GSP-2 in *gfp::par-2* embryos (Fig 4). In these conditions, depletion of SDS-22, whether alone or
446 in conjunction with GSP-1 or GSP-2, results in a partial loss of the PP1 catalytic subunits (GSP-1 or/and
447 GSP-2). This results not in a complete loss but in a reduction in GSP-1/-2 activity, which in turn causes
448 the PAR-2 domain to shrink to some extent.
449 How SDS-22 maintains PP1 level has not been fully clarified. In budding yeast, it has been reported
450 that when Sds22 is mutated, PP1/Glc7 forms aggregates in the nucleus, despite the overall protein level
451 remaining unaltered (Peggie *et al.*, 2002). These aggregates co-localize with heat-shock proteins that
452 require clearance by the proteasome (Cheng & Chen, 2015). Co-expression of PP1 with chaperones
453 GroEL/ES(HSP-60) in bacteria (Peti *et al*, 2013) or with SDS22 in mammalian cells (Choy *et al*, 2019)
454 increases PP1 yield and solubility. These findings suggest that in the absence of SDS22, PP1 is prone
455 to mislocalization or misfolding, leading to aggregation. Interestingly, Peel et al. found SDS-22 co-
456 immunoprecipitated with TCP-1 and HSP-60 (Peel *et al.*, 2017), both members of the chaperonin family
457 critical for protein folding (Hayer-Hartl *et al*, 2016; Kubota *et al*, 1995). Collectively, these findings
458 suggest that by facilitating protein folding SDS22 protects PP1 from degradation. In the *C. elegans*
459 germline and embryos GSP-1/-2 do not form visible aggregates when SDS-22 is depleted but they
460 undergo degradation in a proteasome-dependent manner (Fig. 7). Our data, together with previous
461 findings (Cao *et al.*, 2024; Cheng & Chen, 2015), demonstrate a role of SDS-22 in protecting PP1s from
462 proteasomal degradation. Interestingly, E153A mutation of SDS-22 affected GSP-2 levels much more
463 strongly than GSP-1 levels in embryos (Fig 6F-H). Furthermore, in germlines, GSP-1 levels were less
464 affected by loss of SDS-22 (Fig 7). This indicates that GSP-2 is more susceptible to the interaction with
465 SDS-22.
466 Our data and the recent studies of the Bollen and Meyer laboratories (Cao *et al.*, 2024; Kueck *et al.*,
467 2024) suggest that there is a canonical regulator of GSP-1 and GSP-2 in embryonic polarity that we
468 have not yet identified. In the immunoprecipitations of GSP-2 from embryos we have identified APE-1
469 and SZY-2(I-2). APE-1 has been shown to direct GSP-2, but not GSP-1, localization to epidermal
470 junctions and modulate GSP-2 activity (Beacham *et al.*, 2022). SZY-2(I-2) regulates both GSP-1/-2 in
471 centriole duplication from the four-cell stage of *C. elegans* embryos (Peel *et al.*, 2017). However, our
472 data suggest that neither APE-1 nor SZY-2 functions as canonical PP1 regulators in PAR-2's regulation,
473 as depletion of either did not rescue the polarity defects of *pkc-3(ne4246)* mutant (Fig 1A, EV2A). We
474 cannot exclude the possibility that SDS-22 may also function as a canonical regulator of the PP1
475 holoenzymes in controlling PAR-2 localization in *C. elegans* embryos. Further investigation is required
476 to determine whether a yet-to-be-identified regulator of the PP1 holoenzyme is responsible for loading
477 PAR-2 to the posterior cortex.
478 Another open question is if and how the activity of PP1 catalytic subunits is asymmetrically modulated
479 in the one-cell embryo. Our previous work (Calvi *et al.*, 2022) suggests that the activity of GSP-1/-2
480 might be asymmetrically restricted by the anterior-enriched polo-like kinase PLK-1, which
481 consequently gives rise to asymmetric posterior localization of PAR-2. One possibility is that PLK-1

482 directly phosphorylates and regulates the activity of GSP-1 and/or GSP-2. Interestingly, a recent study
483 shows that in *Drosophila* cells POLO kinase phosphorylates and inhibits PP1 (Moura *et al*, 2024).
484 However, we were not able to identify any potential phosphorylated site that regulates PP1 activity (our
485 unpublished data). Another possibility is that PLK-1 regulates the regulatory subunit(s) of GSP-1/-2.
486 Notably, in mammalian cells, SDS22 is phosphorylated and inhibited by Plk1 during mitosis (Duan *et*
487 *al.*, 2016). Further studies will be required to understand whether additional pathways regulate the
488 activity of this phosphatase during polarity establishment.
489

490 **Material and Methods**
491

492 **Worm strains**

493 Worms were maintained on NGM plates seeded with OP50 bacteria using standard methods (Brenner,
494 1974). The strains used in this work are listed in Table S1. The strains containing the temperature
495 sensitive *pkc-3(ne4246)* mutation, *pkc-3(ne4246); gfp::par-2* (Ng *et al*, 2022) and *pkc-3(ne4246);*
496 *gfp::par-2; sds-22(E153A),* were kept at 15°C. All the other strains were maintained at 20°C.
497 Mutant strains were generated using CRISPR/Cas9 technology as described (Arribere *et al*, 2014). The
498 single guide RNAs, repair templates used to generate the mutants, PCR primers used to amplify the
499 sequence with mutation, as well as enzymes used for the screening, are listed in Table S2-4. For the
500 strain ZU341 *(gfp::par-2; sds-22(E153A))*, two independent isolates were analyzed. The ZU362
501 *mNG::gsp-2; sds-22(E153A)* was maintained as a *sds-22(E153A)* heterozygote. *mNG::gsp-2; sds-*
502 *22(E153A)* adult worms are viable but produce 100% dead progeny, indicating that this mutation
503 behaves as a maternal effect lethal in the *mNG::gsp-2* background.
504

505 **RNA interference**

506 Clones from the Ahringer feeding library (Ahringer, 2006; Kamath *et al*, 2003) were used as listed in
507 Table S5. The clone C06A6.2 served as the control for the injection experiments, as previously done
508 (Bondaz *et al*, 2019). A fragment of APE-1 was amplified from cDNA and cloned into the final pDEST-
509 L4440 vector using Gateway technology (primer listed in Table S5). Double-stranded RNA (dsRNA)
510 for injections was produced with the Promega Ribomax RNA production system.
511 dsRNA was injected in L4/young adult hermaphrodites, which were then incubated at 20°C. For the co-
512 depletion of SDS-22 and GSP-1/-2, and co-depletion of GSP-1 and GSP-2, a mixture of 1:1 dsRNAs
513 was injected (Fig 4, Fig EV5, EV7). Embryos from injected worms were analyzed 16-20 hours after
514 injection.
515 RNA interference by feeding was performed on plates containing 1mM IPTG. The L4440 vector was
516 used as control. For the *pkc-3(ne4246)* strains and controls, worms were incubated on feeding plates at
517 semi-restrictive temperatures of 24°C (Fig 1, Fig 3D, Fig EV2A) or 22°C (Fig 3E,F,G). L4 larvae were
518 added to RNAi feeding plates and incubated for 24 hours. For co-depletion of SDS-22 and RPN-6.1/-7

519 (Fig7, EV8-9), a mixture of 1:1 fresh bacteria culture was plated. Worms were incubated on feeding
520 plates at 20°C for 24h hours (Fig 5A, Fig 6A-E, Fig7, EV2B, EV3, EV8-9).
521
522 **Immunoprecipitation and mass spectrometry**
523 For immunoprecipitation experiments from embryos of mNeonGreen tagged GSP-2, worms were
524 grown in 3X PEP plates and embryos were harvested from gravid worms by bleaching (500 mM NaOH
525 and 5% bleach). The *N2* strain was used as a control. The mNeonGreen::GSP-2 and control
526 immunoprecipitations were performed in triplicate. Packed embryos were frozen in liquid nitrogen and
527 stored at −80°C. Embryos were then thawed, resuspended in immunoprecipitation buffer (100 mM KCl,
528 50 mM Tris (pH: 7.5), 1 mM MgCl2, 1 mM DTT, 5% glycerol, 0.2% NP-40, 1 mM EDTA, and protease
529 and phosphatase inhibitor cocktail (Roche)). The embryos were ground using a mill (Retsch MM301)
530 and silica beads (Lysing matrix C, MP Biomedicals). The protein homogenate was centrifuged at 14,000
531 rpm for 30 min at 4°C. The protein concentration in the supernatant was determined in a Bradford assay
532 (Bio-Rad Laboratories) using a UV/Vis Spectrophotomer (Labgene scientific). About 3 mg of
533 embryonic extract was incubated at 4°C for 1.5 h with 10 µl of mNeonGreen-Trap Agarose beads
534 (Chromotek), previously washed 3 times with IP buffer. After the incubation with the embryonic extract,
535 beads were washed three times with IP buffer, and three times with the buffer containing 100 mM KCl,
536 50 mM Tris (pH: 7.5), 1 mM MgCl2, 1 mM DTT, 1 mM EDTA to remove nonspecific binding. Elution
537 of mNeonGreen-tagged GSP-2 was performed by incubation of the beads for 10min at room
538 temperature with 25 µl of 0.15% TFA. The pH of the elution was corrected to pH: 7-8 with 0.5M Tris
539 (pH:7.9). 3 µl of the elutions were used to analyse the immunoprecipitation by western blot. 22 µl of
540 the elutions were snap frozen and sent to Biognosys (https://biognosys.com) for mass spectrometric
541 analysis. The elutions were subjected to denaturation, reduction, alkylation, digestion and C18 clean up.
542 The peptide digests were acquired in DIA mode using an Orbitrap Exploris 480 (Thermo Fisher) and
543 analyzed with directDIA (Spectronaut 15).
544
545 **Imaging of live embryos**
546 Adult hermaphrodites were dissected on a coverslip in a drop of Egg Buffer (118 mM NaCl, 48 mM
547 KCl, 2 mM $CaCl_2$, 2 mM $MgCl_2$, and 25 mM Hepes, pH 7.5). Embryos were mounted on a 3% agarose
548 pad for imaging. Time-lapse recordings, with frames captured every 10 seconds, were conducted using
549 a Nikon ECLIPSE Ni-U microscope equipped with a Nikon DS-U3 Digital Camera and a 60X/1.25
550 numerical aperture (NA) objective. Imaging was performed between 20 - 22°C.
551
552 **Immunostaining and imaging of fixed embryos**
553 Fixation and staining of embryos were carried out as described previously (Calvi *et al.*, 2022). The
554 primary antibody phospho-Histone 3 (Ser10) (Millipore, rabbit) was diluted 1:500 in PBST with 1%
555 BSA and slides incubated overnight at 4°C. Slides were then washed and incubated with the secondary

556 antibody (4 µg/ml Alexa Fluor 568–coupled anti-rabbit antibody) and 1 µg/ml DAPI to visualize DNA.
557 Images were acquired using a Nikon ECLIPSE Ni-U microscope, equipped with a Nikon DS-U3 Digital
558 Camera, and using a 60X/1.25 numerical aperture (NA) objective.
559
560 **Embryonic lethality**
561 To assess the embryonic lethality, young adult worms were singled on NGM plates seeded with OP50
562 and incubated at 20°C for 24 hours. Adults were the removed and the plates were incubated for an
563 additional 24 hours at 20°C (Fig 3C, Fig EV6, and other *sds-22(E153A)* mutants in *N2* and in *sds-*
564 *22::gfp* genetic backgrounds). To quantify the lethality of *mNG::gsp-2; sds-22(E153A)* strain, which
565 was maintained as a *sds-22(E153A)* heterozygote, L4/young adult worms (homozygote wild-type,
566 heterozygote, or homozygote *sds-22(E153A)* mutant) were singled on OP50 seeded-NGM plates,
567 allowed to lay eggs for 24 hours, and subsequently lysed for genotyping. Homozygote *sds-22* wild-type
568 and heterozygote worms expressing wildtype *sds-22* from one allele and mutant *sds-22(E153A)* from
569 the other allele were used as a control. SDS-22(E153A) mutation in wildtype *N2* exhibited 8.3% of
570 lethality, while *sds-22(E153A)::gfp* showed a lethality of 51.9%.
571 For the RNAi feeding and lethality assay of *pkc-3(ne4246)* mutant, L4 worms were initially transferred
572 to 1mM IPTG plates seeded with feeding bacteria and incubated overnight at 15°C. The following day,
573 young adult worms were singled onto feeding plate and incubated for 24 hours at 24°C (Fig 1A, 3D)
574 and 22°C (Fig 3E). After this period, the adult worms were removed and the plates were further
575 incubated at 24°C and 22°C respectively for 24 hours. The ratio of unhatched embryos to the total F1
576 progeny (unhatched embryos plus larvae) was used to calculate the percentage of embryonic lethality.
577
578 **Yeast two-hybrid assay**
579 The interaction between SDS-22 and GSP-1/-2 was assessed using a GAL4-based yeast two-hybrid
580 (Y2H) system (Gateway, Invitrogen) using the MAV203 yeast strain. Full-length SDS-22 (1-326)
581 fragments, both wild type and mutant (E153A), were fused to the GAL4 DNA binding domain (DBD,
582 Bait plasmid). Full-length cDNAs of GSP-1 and GSP-2 were fused to the GAL4 activation domain (AD,
583 Prey plasmid). The SDS-22 wild type and mutant fragments, GSP-1 and GSP-2 were first cloned into
584 the pDONR201, then transferred to the pDEST32 (GAL4DBD) and pDEST22 vector (GAL4AD)
585 separately using Gateway technology. Mutations were introduced by Pfu site-directed mutagenesis. A
586 list of plasmids and primers used for the Y2H assay is provided in Table S6 and S7 respectively.
587 Transformants were selected on synthetic defined (SD) medium lacking leucine and tryptophan.
588 Interactions were tested by spotting single colonies containing the desired plasmids on medium lacking
589 leucine, tryptophan and histidine, with 7.5mM of 3AT (3-amino-1,2,3- triazole, Sigma). Picture of the
590 plates were captured using the Fusion FX6 EDGE Imaging System (Vilber) equipped with an Evo-6
591 Scientific Grade CCD camera.
592

593 **Western blot**
594 Embryos obtained by hypochlorite treatment from two 5cm plates of adult worms were resuspended in
595 SDS sample buffer and denatured at 95°C for 5 minutes. Approximately 3000 embryos per sample were
596 loaded onto a 10% SDS-PAGE gel, followed by Western blotting with ECL detection (Vilber, Fusion
597 FX). Primary antibodies [(anti-TUBULIN (1/2500, mouse, Sigma), anti-mNeonGreen (1/1000, mouse,
598 ChromoTek) and anti-GFP (1/2500, rabbit, Pines)] were incubated overnight at 4°C. HRP-conjugated
599 secondary antibodies were incubated for 45 minutes at room temperature.
600 Band signal measurement for anti-TUBULIN, anti-mNeonGreen, and anti-GFP was performed in Fiji
601 ImageJ by drawing equal-sized ROIs over each band. Mean intensity values were used for
602 quantification, and background was subtracted using the mean intensity of an equivalent ROI placed
603 below the band of interest. The ratio of *ctrl(RNAi)* treatment was normalized to 1.
604
605 **Image analysis and measurement**
606 *Cortical PAR-2 size measurement (Fig 1C, Fig 3B, Fig 4)*
607 The size of cortical GFP::PAR-2 domain was determined by measuring the length of the PAR-2 domain
608 normalized for the total perimeter of the embryo at pronuclear meeting. The perimeter of the embryo
609 and the length of the PAR-2 domain were measured by the Qupath software with machine learning, as
610 detailed previously (Vaudano *et al*, 2024). The length of the PAR-2 domain is represented as a
611 percentage of the total perimeter of the embryo.
612
613 *Cortical PAR-2 intensity measurement (Fig 3F,G)*
614 The line file of GFP::PAR-2 intensity along the whole cortex was measured in one-cell stage embryos
615 at pronuclear meeting. Using ImageJ software, a free-line 5-pixel-wide was positioned at the anterior
616 pole of the cortex (position 0 µm) and traced manually along the whole cortex to the posterior pole
617 (position 75 µm) and back to the anterior pole. The background was subtracted from each value. The
618 intensity of the line profile (from 0 to 75 µm) of the segment traced was shown in an arbitrary unit (a.u.).
619 Images were in 16-bit format.
620
621 *AB cell size measurement (Fig 1D,E)*
622 The total length of the embryo was measured manually from the anterior to the posterior pole using
623 ImageJ software. AB cell size was measured from the anterior pole to the cleavage midline when the
624 embryo just divided into two cells. The AB cell ratio was calculated as the proportion of AB cell size
625 relative to the total embryo length (AB cell plus P1 cell length).
626
627 *Protein intensity of mNG::GSP-2, GFP::GSP-1, SDS-22::GFP in embryos and germlines (Fig 6-7, Fig*
628 *EV4, Fig EV7-9)*

For embryos, the mean intensity of cytoplasmic mNG::GSP-2, GFP::GSP-1, SDS-22::GFP was determined by tracing a fixed-length line in the cytoplasm from the anterior to the posterior of the embryo (above the nucleus) at pronuclear meeting stage using the ImageJ software. The background was subtracted from each value.

For the embryonic intensity of mNG::GSP-2 in the *sds-22(E153A)* mutant genetic background, which is embryonic lethal, L4/young adult worms (homozygote wild type, heterozygote or homozygote mNG::GSP-2; sds-22(E153A) mutant) were singled, let them lay few eggs, and subsequently dissected for imaging. Homozygous *mNG::GSP-2; sds-22(E153A)* mutant worms were recognized by looking at the progeny in the original plates, as homozygote *mNG::GSP-2; sds-22(E153A)* worms only lay dead eggs. Homozygote *sds-22* wild-type and heterozygote worms expressing wildtype *sds-22* from one allele and mutant *sds-22(E153A)* from the other allele were used as a control.

For germlines, mean cytoplasmic and nuclear intensities of mNG::GSP-2, GFP::GSP-1, SDS-22::GFP were measured by drawing a fixed circle in the cytoplasm and/-or nucleus of -1 and -2 oocytes using ImageJ. Background intensity was subtracted. The mean intensities of the cytoplasmic and nuclear regions in -1 and -2 oocytes were calculated and reported.

The germline intensity of mNG::GSP-2 in the *sds-22(E153A)* mutant cannot be measured because there were no viable embryos after depletion of RNP-6.1 or RNP-7, therefore the genotype of homozygous *mNG::gsp-2; sds-22(E153A)* (also embryonic lethal) cannot be differentiated from the homozygote wild type and heterozygote.

Phospho-Histone 3 (Ser10) intensity measurement (Fig 5)

One-cell stage embryos at anaphase were analyzed. A segment 5-pixel-wide and of constant length, centered at the chromosomes was traced using ImageJ software. For each embryo, the average of three segments (upper, center, and lower chromosomes) was used for quantification. The intensity of the line profile of each embryo was normalized to the average of the value in the cytoplasm at position 0 of the segment traced. The mean intensities of the phospho-Histone 3 (Ser10) on the chromosomes were calculated and reported.

Statistical analysis

Statistical analysis was conducted using GraphPad Prism 9. Details on the statistical tests, sample sizes, number of replicates, and interpretation of error bars are specified in each figure legend, within the results section, or in the methods section, and summarized in Table S8. Data was assumed to have normal distribution.

Significance was defined as: ns, $p > 0.05$, *$p < 0.05$, **$p < 0.01$, ***$p < 0.001$, ****$p < 0.0001$.

Data availability

All the strains and reagents generated in this study are available from the corresponding author upon request. All raw data associated with the experiments will be deposited in Yareta at publication.

Author Contributions

Yi Li: Conceptualization; Formal analysis; Investigation; Visualization; Writing-original draft; Writing-review and editing. Ida Calvi: Conceptualization; Investigation; Writing-review and editing. Monica Gotta: Conceptualization; Funding acquisition; Supervision; Writing-original draft; Writing-review and editing

Funding

This research was funded in part by the Swiss National Science Foundation (SNSF) (grant number 31003A_175850). For the purpose of Open Access, a CC BY public copyright licence is applied to any Author Accepted Manuscript (AAM) version arising from this submission.

Disclosure and competing interest statement

The authors declare no competing or financial interests.

Acknowledgments

A special thanks to Erik Griffin, and Dhanya Cheerambathur for strains. We would like to thank all the present and past members of the Gotta, Meraldi and Steiner laboratories, Patrick Meraldi and Florian Steiner for discussions and suggestions. Thanks to Sofia Barbieri, Victoria von Glasenapp and Florian Steiner for comments on the manuscript. Some strains were provided by the CGC, which is funded by NIH Office of Research Infrastructure Programs (P40 OD010440). This research was funded by the Swiss National Science Foundation (grant number 31003A_175850) and the University of Geneva.

References

Aggen JB, Nairn AC, Chamberlin R (2000) Regulation of protein phosphatase-1. *Chem Biol* 7: R13-23

Ahringer J (2006) *Reverse Genetics. WormBook: The Online Review of C. elegans Biology [Internet]. WormBook; 2005-2018.*

Arribere JA, Bell RT, Fu BX, Artiles KL, Hartman PS, Fire AZ (2014) Efficient marker-free recovery of custom genetic modifications with CRISPR/Cas9 in Caenorhabditis elegans. *Genetics* 198: 837-846

Beacham GM, Wei DT, Beyrent E, Zhang Y, Zheng J, Camacho MMK, Florens L, Hollopeter G (2022) The Caenorhabditis elegans ASPP homolog APE-1 is a junctional protein phosphatase 1 modulator. *Genetics* 222

Billmyre KK, Doebley AL, Spichal M, Heestand B, Belicard T, Sato-Carlton A, Flibotte S, Simon M, Gnazzo M, Skop A *et al* (2019) The meiotic phosphatase GSP-2/PP1 promotes germline immortality and small RNA-mediated genome silencing. *PLoS Genet* 15: e1008004

Bondaz A, Cirillo L, Meraldi P, Gotta M (2019) Cell polarity-dependent centrosome separation in the C. elegans embryo. *J Cell Biol* 218: 4112-4126

708 Brenner S (1974) The genetics of Caenorhabditis elegans. *Genetics* 77: 71-94
709 Calvi I, Schwager F, Gotta M (2022) PP1 phosphatases control PAR-2 localization and polarity
710 establishment in C. elegans embryos. *J Cell Biol* 221
711 Campanale JP, Sun TY, Montell DJ (2017) Development and dynamics of cell polarity at a glance. *J*
712 *Cell Sci* 130: 1201-1207
713 Cao X, Lake M, Van der Hoeven G, Claes Z, Del Pino Garcia J, Lemaire S, Greiner EC, Karamanou S,
714 Van Eynde A, Kettenbach AN *et al* (2024) SDS22 coordinates the assembly of holoenzymes from
715 nascent protein phosphatase-1. *Nat Commun* 15: 5359
716 Cao X, Lemaire S, Bollen M (2022) Protein phosphatase 1: life-course regulation by SDS22 and
717 Inhibitor-3. *FEBS J* 289: 3072-3085
718 Ceulemans H, Bollen M (2004) Functional diversity of protein phosphatase-1, a cellular economizer
719 and reset button. *Physiol Rev* 84: 1-39
720 Ceulemans H, Vulsteke V, De Maeyer M, Tatchell K, Stalmans W, Bollen M (2002) Binding of the
721 concave surface of the Sds22 superhelix to the alpha 4/alpha 5/alpha 6-triangle of protein phosphatase-
722 1. *J Biol Chem* 277: 47331-47337
723 Cheng YL, Chen RH (2015) Assembly and quality control of the protein phosphatase 1 holoenzyme
724 involves the Cdc48-Shp1 chaperone. *J Cell Sci* 128: 1180-1192
725 Choy MS, Moon TM, Ravindran R, Bray JA, Robinson LC, Archuleta TL, Shi W, Peti W, Tatchell K,
726 Page R (2019) SDS22 selectively recognizes and traps metal-deficient inactive PP1. *Proc Natl Acad*
727 *Sci U S A* 116: 20472-20481
728 Duan H, Wang C, Wang M, Gao X, Yan M, Akram S, Peng W, Zou H, Wang D, Zhou J *et al* (2016)
729 Phosphorylation of PP1 Regulator Sds22 by PLK1 Ensures Accurate Chromosome Segregation. *J Biol*
730 *Chem* 291: 21123-21136
731 Eiteneuer A, Seiler J, Weith M, Beullens M, Lesage B, Krenn V, Musacchio A, Bollen M, Meyer H
732 (2014) Inhibitor-3 ensures bipolar mitotic spindle attachment by limiting association of SDS22 with
733 kinetochore-bound protein phosphatase-1. *EMBO J* 33: 2704-2720
734 Fernando LM, Quesada-Candela C, Murray M, Ugoaru C, Yanowitz JL, Allen AK (2022) Proteasomal
735 subunit depletions differentially affect germline integrity in C. elegans. *Front Cell Dev Biol* 10: 901320
736 Goehring NW (2014) PAR polarity: from complexity to design principles. *Exp Cell Res* 328: 258-266
737 Goldstein B, Macara IG (2007) The PAR proteins: fundamental players in animal cell polarization. *Dev*
738 *Cell* 13: 609-622
739 Grusche FA, Hidalgo C, Fletcher G, Sung HH, Sahai E, Thompson BJ (2009) Sds22, a PP1 phosphatase
740 regulatory subunit, regulates epithelial cell polarity and shape [Sds22 in epithelial morphology]. *BMC*
741 *Dev Biol* 9: 14
742 Hao Y, Boyd L, Seydoux G (2006) Stabilization of cell polarity by the C. elegans RING protein PAR-
743 2. *Dev Cell* 10: 199-208
744 Hayer-Hartl M, Bracher A, Hartl FU (2016) The GroEL-GroES Chaperonin Machine: A Nano-Cage
745 for Protein Folding. *Trends Biochem Sci* 41: 62-76
746 Heroes E, Van der Hoeven G, Choy MS, Garcia JDP, Ferreira M, Nys M, Derua R, Beullens M, Ulens
747 C, Peti W *et al* (2019) Structure-Guided Exploration of SDS22 Interactions with Protein Phosphatase
748 PP1 and the Splicing Factor BCLAF1. *Structure* 27: 507-518 e505
749 Hsu JY, Sun ZW, Li X, Reuben M, Tatchell K, Bishop DK, Grushcow JM, Brame CJ, Caldwell JA,
750 Hunt DF *et al* (2000) Mitotic phosphorylation of histone H3 is governed by Ipl1/aurora kinase and
751 Glc7/PP1 phosphatase in budding yeast and nematodes. *Cell* 102: 279-291
752 Kamath RS, Fraser AG, Dong Y, Poulin G, Durbin R, Gotta M, Kanapin A, Le Bot N, Moreno S,
753 Sohrmann M *et al* (2003) Systematic functional analysis of the Caenorhabditis elegans genome using
754 RNAi. *Nature* 421: 231-237
755 Kapoor S, Kotak S (2019) Centrosome Aurora A regulates RhoGEF ECT-2 localisation and ensures a
756 single PAR-2 polarity axis in C. elegans embryos. *Development* 146
757 Klinkert K, Levernier N, Gross P, Gentili C, von Tobel L, Pierron M, Busso C, Herrman S, Grill SW,
758 Kruse K *et al* (2019) Aurora A depletion reveals centrosome-independent polarization mechanism in
759 Caenorhabditis elegans. *Elife* 8
760 Kubota H, Hynes G, Willison K (1995) The chaperonin containing t-complex polypeptide 1 (TCP-1).
761 Multisubunit machinery assisting in protein folding and assembly in the eukaryotic cytosol. *Eur J*
762 *Biochem* 230: 3-16

763 Kueck AF, van den Boom J, Koska S, Ron D, Meyer H (2024) Alternating binding and p97-mediated
764 dissociation of SDS22 and I3 recycles active PP1 between holophosphatases. *Proc Natl Acad Sci U S*
765 *A* 121: e2408787121
766 Lang CF, Munro E (2017) The PAR proteins: from molecular circuits to dynamic self-stabilizing cell
767 polarity. *Development* 144: 3405-3416
768 Lesage B, Beullens M, Pedelini L, Garcia-Gimeno MA, Waelkens E, Sanz P, Bollen M (2007) A
769 complex of catalytically inactive protein phosphatase-1 sandwiched between Sds22 and inhibitor-3.
770 *Biochemistry* 46: 8909-8919
771 Llense F, Etienne-Manneville S (2015) Front-to-Rear Polarity in Migrating Cells. In: *Cell Polarity 1:*
772 *Biological Role and Basic Mechanisms*, Ebnet K. (ed.) pp. 115-146. Springer International Publishing:
773 Cham
774 Longhini KM, Glotzer M (2022) Aurora A and cortical flows promote polarization and cytokinesis by
775 inducing asymmetric ECT-2 accumulation. *Elife* 11
776 MacKelvie SH, Andrews PD, Stark MJ (1995) The Saccharomyces cerevisiae gene SDS22 encodes a
777 potential regulator of the mitotic function of yeast type 1 protein phosphatase. *Mol Cell Biol* 15: 3777-
778 3785
779 Meiselbach H, Sticht H, Enz R (2006) Structural analysis of the protein phosphatase 1 docking motif:
780 molecular description of binding specificities identifies interacting proteins. *Chem Biol* 13: 49-59
781 Moreira S, Osswald M, Ventura G, Goncalves M, Sunkel CE, Morais-de-Sa E (2019) PP1-Mediated
782 Dephosphorylation of Lgl Controls Apical-basal Polarity. *Cell Rep* 26: 293-301 e297
783 Motegi F, Zonies S, Hao Y, Cuenca AA, Griffin E, Seydoux G (2011) Microtubules induce self-
784 organization of polarized PAR domains in Caenorhabditis elegans zygotes. *Nat Cell Biol* 13: 1361-1367
785 Moura M, Barbosa J, Pinto I, Leça N, Cunha-Silva S, Verza AE, Pedroso PD, Lemaire S, Duro J, Silva
786 M *et al* (2024) POLO kinase inhibits Protein Phosphatase 1 to promote the Spindle Assembly
787 Checkpoint and prevent aneuploidy. *bioRxiv*: 2024.2012.2023.630043
788 Munro E, Nance J, Priess JR (2004) Cortical flows powered by asymmetrical contraction transport PAR
789 proteins to establish and maintain anterior-posterior polarity in the early C. elegans embryo. *Dev Cell*
790 7: 413-424
791 Ng K, Bland T, Hirani N, Goehring NW (2022) An analog sensitive allele permits rapid and reversible
792 chemical inhibition of PKC-3 activity in C. elegans. *MicroPubl Biol* 2022
793 Papaevgeniou N, Chondrogianni N (2014) The ubiquitin proteasome system in Caenorhabditis elegans
794 and its regulation. *Redox Biol* 2: 333-347
795 Pedelini L, Marquina M, Arino J, Casamayor A, Sanz L, Bollen M, Sanz P, Garcia-Gimeno MA (2007)
796 YPI1 and SDS22 proteins regulate the nuclear localization and function of yeast type 1 phosphatase
797 Glc7. *J Biol Chem* 282: 3282-3292
798 Peel N, Iyer J, Naik A, Dougherty MP, Decker M, O'Connell KF (2017) Protein Phosphatase 1 Down
799 Regulates ZYG-1 Levels to Limit Centriole Duplication. *PLoS Genet* 13: e1006543
800 Peggie MW, MacKelvie SH, Bloecher A, Knatko EV, Tatchell K, Stark MJ (2002) Essential functions
801 of Sds22p in chromosome stability and nuclear localization of PP1. *J Cell Sci* 115: 195-206
802 Peti W, Nairn AC, Page R (2013) Structural basis for protein phosphatase 1 regulation and specificity.
803 *FEBS J* 280: 596-611
804 Posch M, Khoudoli GA, Swift S, King EM, Deluca JG, Swedlow JR (2010) Sds22 regulates aurora B
805 activity and microtubule-kinetochore interactions at mitosis. *J Cell Biol* 191: 61-74
806 Qian J, Lesage B, Beullens M, Van Eynde A, Bollen M (2011) PP1/Repo-man dephosphorylates mitotic
807 histone H3 at T3 and regulates chromosomal aurora B targeting. *Curr Biol* 21: 766-773
808 Riga A, Castiglioni VG, Boxem M (2020) New insights into apical-basal polarization in epithelia. *Curr*
809 *Opin Cell Biol* 62: 1-8
810 Rodrigues NT, Lekomtsev S, Jananji S, Kriston-Vizi J, Hickson GR, Baum B (2015) Kinetochore-
811 localized PP1-Sds22 couples chromosome segregation to polar relaxation. *Nature* 524: 489-492
812 Santoro A, Vlachou T, Carminati M, Pelicci PG, Mapelli M (2016) Molecular mechanisms of
813 asymmetric divisions in mammary stem cells. *EMBO Rep* 17: 1700-1720
814 Stone EM, Yamano H, Kinoshita N, Yanagida M (1993) Mitotic regulation of protein phosphatases by
815 the fission yeast sds22 protein. *Curr Biol* 3: 13-26

Tzur YB, Egydio de Carvalho C, Nadarajan S, Van Bostelen I, Gu Y, Chu DS, Cheeseman IM, Colaiacovo MP (2012) LAB-1 targets PP1 and restricts Aurora B kinase upon entrance into meiosis to promote sister chromatid cohesion. *PLoS Biol* 10: e1001378

Vaudano AP, Schwager F, Gotta M, Barbieri S (2024) Internal feedback circuits among MEX-5, MEX-6, and PLK-1 maintain faithful patterning in the Caenorhabditis elegans embryo. *Proc Natl Acad Sci U S A* 121: e2407517121

Verbinnen I, Ferreira M, Bollen M (2017) Biogenesis and activity regulation of protein phosphatase 1. *Biochem Soc Trans* 45: 89-99

Virshup DM, Shenolikar S (2009) From promiscuity to precision: protein phosphatases get a makeover. *Mol Cell* 33: 537-545

Wurzenberger C, Held M, Lampson MA, Poser I, Hyman AA, Gerlich DW (2012) Sds22 and Repo-Man stabilize chromosome segregation by counteracting Aurora B on anaphase kinetochores. *J Cell Biol* 198: 173-183

Xin G, Fu J, Luo J, Deng Z, Jiang Q, Zhang C (2020) Aurora B regulates PP1gamma-Repo-Man interactions to maintain the chromosome condensation state. *J Biol Chem* 295: 14780-14788

Zhao P, Teng X, Tantirimudalige SN, Nishikawa M, Wohland T, Toyama Y, Motegi F (2019) Aurora-A Breaks Symmetry in Contractile Actomyosin Networks Independently of Its Role in Centrosome Maturation. *Dev Cell* 48: 631-645 e636

Supplementary movies

Movie EV1: *sds-22(RNAi)* rescues PAR-2 posterior cortical localization in the *pkc-3(ne4246); gfp::par-2* embryos.

gfp::par-2 and *pkc-3*(*ne4246*); *gfp::par-2* embryos treated either with *ctrl*(*RNAi*) or *sds-22*(*RNAi*) (RNAi by feeding). Acquisition of midplane fluorescent images begins during the early establishment phase, and frames are captured every 10 s. In *gfp::par-2* embryos (both *ctrl*(*RNAi*) and *sds-22*(*RNAi*)) PAR-2 localizes at the posterior cortex in the one-cell stage embryo and in P1 in the two-cell stage embryo (n = 12 for both). In *pkc-3*(*ne4246*); *gfp::par-2*, *ctrl*(*RNAi*) PAR-2 is uniformly distributed at the cortex in both one- and two-cell stage embryo (n = 42). After depletion of SDS-22, *pkc-3*(*ne4246*); *gfp::par-2* embryos showed PAR-2 posterior localization in one-cell stage embryo and in the P1 cell (n = 42 out of 48). N = 5. n = number of embryos analyzed; N = number of independent experiments. Anterior is to the left and posterior to the right. Referred to Fig 1B.

Movie EV2: *sds-22*(*E153A*) substitution reduces the length of the PAR-2 cortical domain.

Acquisition of midplane fluorescent images begins during the early stage, and frames are captured every 10 s. In *gfp::par-2; sds-22(E153A)* mutant embryos the length of cortical PAR-2 domain is decreased compared to *gfp::par-2* embryos at pronuclear meeting stage (n = 30 and n = 52, respectively). N = 3. n = number of embryos analyzed. N = number of independent experiments. Anterior is to the left and posterior to the right. Referred to Fig 3A,B.

Movie EV3: *sds-22*(*E153A*) substitution rescues PAR-2 posterior cortical localization in the *pkc-3*(*ne4246*); *gfp::par-2* embryos at 22°C.

858 Acquisition of midplane fluorescent images begins during the early stage, and frames are captured
859 every 10 s. In *gfp::par-2; pkc-3*(*ne4246*); *sds-22(E153A)* mutant embryos PAR-2 is more enriched to
860 the posterior cortex compared to *gfp::par-2; pkc-3*(*ne4246*) embryos where PAR-2 is localized all
861 over the cortex (n = 19 for both genotypes). N = 3. n = number of embryos analyzed. N = number of
862 independent experiments. Anterior is to the left and posterior to the right. Referred to Fig 3F,G.
863
864
865
866
867
868